Journal of Constructional Steel Research 66 (2010) 399–405

Contents lists available at ScienceDirect

Journal of Constructional Steel Research

journal homepage: www.elsevier.com/locate/jcsr

Application of fire-resistant steel to beam-to-column moment connections at elevated temperatures

Hsin-Yang Chung *, Chen-Hung Lee, Wun-Jie Su, Rih-Zeng Lin

Department of Civil Engineering, National Cheng Kung University, Tainan 701, Taiwan

ARTICLE INFO

Article history:
Received 23 October 2008
Accepted 29 September 2009

Keywords:
Fire-resistant steel
Fire test
Moment connection
Elevated temperature
Finite element analysis

ABSTRACT

This paper presents a new method of using fire-resistant steel to improve the fire-resistance of beam-to-column moment connections in steel structures. Two full-scale beam-to-column moment connection specimens were tested at elevated temperatures according to the standard ISO-834 fire to verify the feasibility of the proposed method. In addition, a detailed 3-D finite element model was developed to simulate the structural behavior of the column-tree moment connection specimens in fire. The fire test results show that the proposed method can effectively extend the fire endurance time, reduce structural deformation, and raise the critical temperature to failure for the beam-to-column moment connections. The numerical results obtained from the 3-D finite element analysis for the two specimens successfully simulated the fire test results.

1. Introduction

In fire conditions, beam-to-column connections play an important role in the structural behavior of steel structures. Due to the degradation of the strength and stiffness of steel at elevated temperatures, whether the connections can sustain large forces and rotations in fire directly affects the ability of the connections to redistribute forces from the beams to other structural members, and influences the survival time of steel structures in fire. Evidence from the WTC building collapses [1,2] demonstrated the importance of connections for steel structures in fire. Many fire scene investigations of steel buildings and the results of the Cardington full-scale eight story steel building fire tests in the UK [3] have also shown how the connections help the structural system survive extreme fires without progressive collapse. Therefore, preventing beam-to-column connections from failing is important for steel structures subjected to fires. Traditionally, to protect steel structures from fire damage, fire-protection materials such as thermal insulation components are required by the prescriptive-based fire protection design method. By applying the prescribed thicknesses of fire-protection material on steel members as surface coatings, the temperatures of steel members can be kept below the specified high temperatures for the given fire durations, and steel members can achieve the fire ratings required by code. However, this traditional method can add 30% to the construction cost of bare steelwork [4] and increase the construction time for steel structures.

In addition to the traditional method, the use of fire-resistant steel, which can retain 2/3 or more of its specified ambient-temperature yield strength at 600 °C, provides an alternative way to improve the fire-resistant ability for components of steel structures. The superior high-temperature mechanical properties of fire-resistant steel have been reported by Sakumoto et al. [5] and Kelly and Shi [6]. Using structural members made of fire-resistant steel can effectively reduce the usage of fire-protection coatings. Moreover, in some special fire conditions in which the steel temperature will not reach 600 °C, structural members made of fire-resistant steel may be exposed to fire without any protection [5]. However, experimental investigations of beam-to-column connections made of fire-resistant steel are rarely reported in literature. This may be due to the difficulty of conducting beam-to-column connection tests and the variety of the connection types. In addition, the cost of fire-resistant steel is still higher than that of conventional steel, so it is important to determine how to use fire-resistant steel economically. Instead of applying fire-resistant steel to all of the structural members, fire-resistant steel could be used only in the parts that are most important or susceptible to fire. The particular design of a column-tree moment-resisting frame (MRF) system makes it possible to use fire-resistant steel to the moment connection portion of the system to improve the fire-resistant performances of beam-to-column moment connections. The column-tree MRF is a common steel construction design used in some high seismic risk regions due to its better quality

* Corresponding author. Tel.: +886 6 2757575x63145; fax: +886 6 2358542.
E-mail address: hychung@mail.ncku.edu.tw (H.-Y. Chung).

0143-974X/$ – see front matter © 2009 Elsevier Ltd. All rights reserved.
doi:10.1016/j.jcsr.2009.09.009

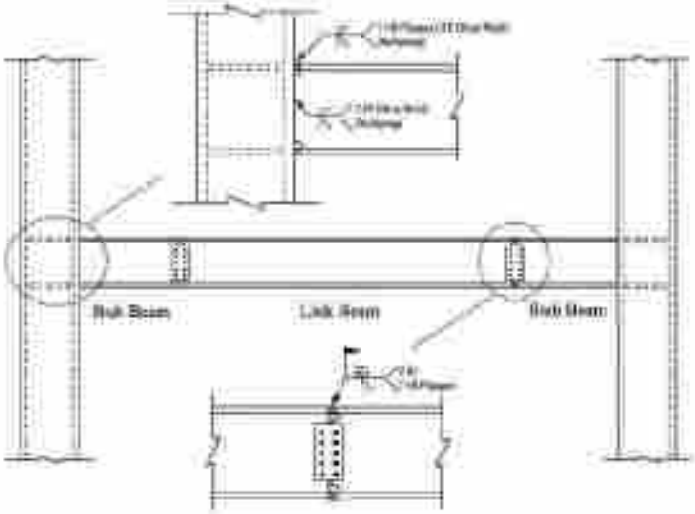

Fig. 1. Part of a typical column-tree moment resisting frame.

control in beam-to-column joint welding and its erection efficiency during construction. Fig. 1 shows the part of a typical column-tree moment-resisting frame in Taiwan. To improve the fire-resistance of the moment connections, we proposed that the stub beams in column trees can be made of fire-resistant steel. The feasibility of this proposal is examined by two full-scale beam-to-column moment connection specimens in the experimental portion of this study.

Several beam-to-column connection fire tests have been conducted in the past to understand the structural behavior of beam-to-column connections at elevated temperatures. Most of these studies focused on the bolted connections, and the specimens were isolated beam-to-column subassemblages [2–6]. Unlike the previous experimental studies using isolated specimens, Ding and Wang [10] utilized complete "rugby goalpost" subassemblage frames to conduct steel beam to concrete-filled tubular column connection tests to four types of connections. This "rugby goalpost" type specimen can provide axial restraint to the beam and simulate the realistic forces applied to a connection. Qian et al. [11] tested six bare steel beam-to-column connection specimens with extended plate connections at three high temperatures (400 °C, 550 °C and 700 °C). Some of the specimens were tested with the beams subjected to various compressive axial forces to simulate axial restraint effects. Yu et al. [12] developed a unique test setup that could apply both shear and tying forces to beams to test 14 beam-to-column specimens with fin plate connections subjected to catenary action at elevated temperatures.

From the previous literature review of beam-to-column connections in fire, it can be seen that most experimental efforts focused on bolted connections and useful data and experiences were obtained to understand the structural behaviors of various bolted beam-to-column connections in fire. The behaviors of welded beam-to-column moment connections, such as column-tree moment connections and the popular flange welded and web bolted moment connections, at elevated temperatures are rarely reported. Therefore, the two objectives of this study are as follows.

(1) Conduct fire tests on full-scale column-tree moment connection specimens to verify the feasibility of the proposed method.
(2) Develop a detailed 3-D FE model to accurately simulate the structural behaviors of the H-beam to box-column column-tree moment connection specimens at elevated temperatures.

2. Test specimens

2.1. Specimen design and fabrication

In order to determine the effect of using fire-resistant steel in the stub beam of a column-tree moment connection, two full-scale column-tree moment connection specimens were fabricated and tested at elevated temperatures for comparison. The two specimens were identical in dimensions, fabrication process, welding procedures, and materials, but different in the steel types used for the stub beams. The stub beam in Specimen #1 was made of fire-resistant steel, while that of Specimen #2 used normal structural steel. Each column-tree moment connection specimen was composed of a column tree (including a stub H-beam and a box-column) and a link H-beam spliced to the stub beam. The design of the column-tree moment connection specimen came from an exterior H-beam to box-column subassemblage of a newly designed and constructed steel building in Taipei, Taiwan. Fig. 2 shows the analogy of a constantly loaded specimen in a heating furnace to simulate an exterior column-tree moment connection of a building in fire. When a steel MRF building is on fire, the beam-to-column moment connections sustain not only moments but also compressive or tensile axial forces due to the responses of the beams to the fire. To resist moments in some high seismic or wind risk areas, a moment connection usually has sufficient strength capacity to resist the tensile axial forces in fire as well. Hence, tensile failures of moment connections are rarely reported in fire scene investigations of steel structures. Instead, local flange buckling or web buckling are the common failure modes for beam-to-column moment connections in fire [1]. In order to simulate the common local buckling failure modes in the fire experiment, a constant vertical load was applied to the H-beam to box-column subassemblage specimen at the cantilevered beam end to approximate a negative moment gradient near the moment connection. It is noted that, in the fire experiment, the two bare specimens were entirely exposed to fire in the furnace without fireproof coatings to simulate the most severe fire condition. Figs. 3 and 4 illustrate the dimensions and welding details of the test specimens, and Table 1 lists the steel types, bolts and weld metals used to fabricate the two specimens. Table 2 lists a summary of the weld metals for all the welding processes (see Fig. 4) utilized

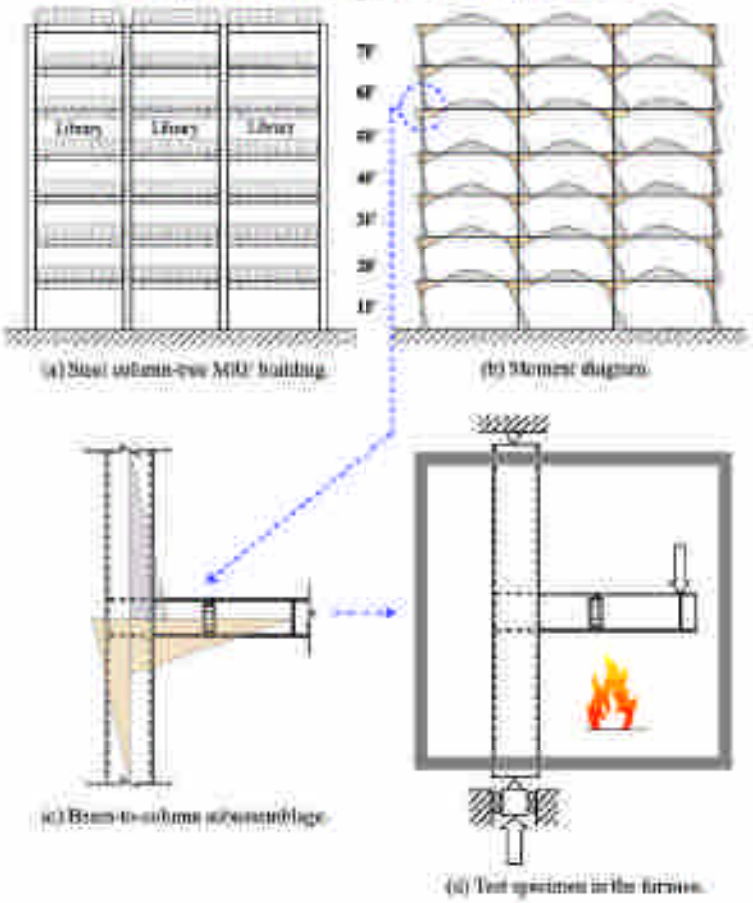

Fig. 2. Test specimen to simulate the moment distribution of an exterior beam-to-column subassemblage in fire.

Table 1
Steel type used in the components of two specimens

Specimen number	Steel type			
	Box column	Stub beam	Link beam	High-strength bolt
#1	SN490B	SN490C-FR	SN490B	S10T
#2	SN490B	SN490B	SN490B	S10T

in specimen fabrication. In particular for Specimen #1, the 0.75 m stub H-beam (BH488 × 300 × 11 × 18) was made of SN490C-FR fire-resistant steel, and the stub H-beam was welded to the box-column using shielded metal arc welding (SMAW) and the matching weld metal of AWS A5.5 E7016-A1 heat-resistant steel electrodes.

2.2. Material properties

Table 3 summarizes yield strength and ultimate strength for steel components of the two specimens from the tensile coupon tests at ambient temperature, and Table 4 summarizes the high temperature reduction factors of yield strength $k_y(T)$, ultimate strength $k_u(T)$, and Young's modulus $k_E(T)$ from 100 °C to 800 °C for JIS SN490B steel, SN490C-FR fire-resistant steel, and JIS S10T high strength bolts provided by the materials lab of the steel provider.

The chemical composition of SN490C-FR steel is listed in Table 5. Molybdenum (Mo), niobium (Nb), and vanadium (V) were purposely added to the SN490C-FR steel to increase the fire-resistance of the steel at high temperatures. The fire-resistance comes from the precipitation-hardening mechanism of molybdenum, niobium, and vanadium carbides to pin down grain boundaries

Table 2
Weld metal used in specimen fabrication

Specimen number	Welding			
	SAW	BSW	ICAW	SMAW
#1	AWS A5.17 F7A2-EM12K	AWS A5.20 E71T-1	AWS A5.20 E71T-1	AWS A5.5 E7016-A1
#2	AWS A5.17 F7A2-EM12K	AWS A5.20 E71T-1	AWS A5.20 E71T-1	

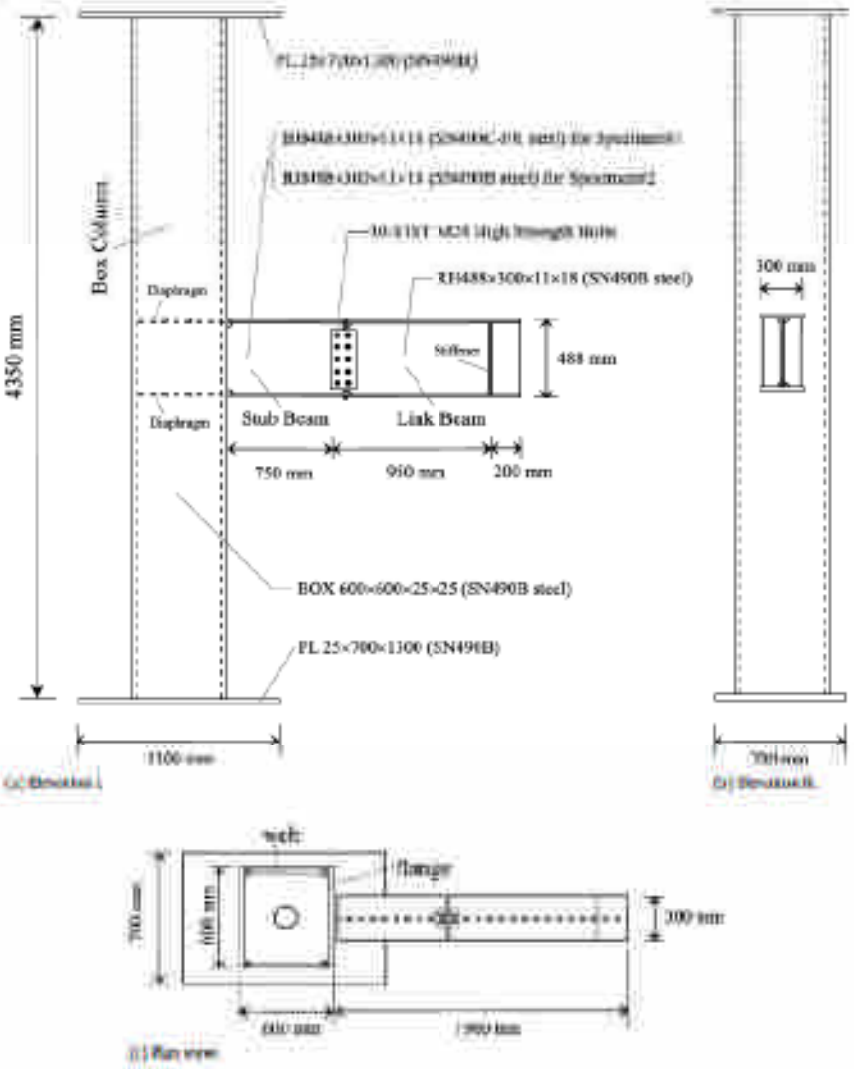

Fig. 3. Dimensions of test specimens.

Table 3
Summary of tensile coupon test results for specimens (specimens at room temperature).

Section & bolt	Coupon location	Steel type	Yield stress F_y (MPa)	Tensile stress F_u (MPa)
RH488 × 300 × 11 × 18	Flange	SN490B	396.6	534.8
	Web	SN490B	476.6	575.4
RH488 × 300 × 11 × 18	Flange	SN490C-FR	448.1	582.7
	Web	SN490C-FR	448.1	582.7
BOX600 × 600 × 25 × 25	Flange	SN490B	396.6	534.8
	Web	SN490B	396.6	534.8
M24 high-strength bolt	Shank	10.9T	981.2	1042.9

and dislocations at high temperatures; this pinning action can delay yielding and prevent creep up to a high target temperature. The target temperature of SN490C-FR steel is 600 °C, at which the fire-resistant steel still possesses 2/3 of its specified yield strength (325 MPa) at an ambient temperature. The material test results summarized in Table 4 show that SN490C-FR steel at the target temperature of 600 °C retains 57% of its ambient yield strength (448.1 MPa), which is greater than 2/3 of the specified yield strength at ambient temperature and reaches the target of fire-resistant steel at 600 °C. In addition, to prevent weld metal failure at elevated temperatures, the stub beam was welded to the box-column flange using the matching weld metal of E7016-A1 heat-resistant carbon–molybdenum steel electrodes. The chemical compositions of the heat-resistant electrodes are shown in Table 6.

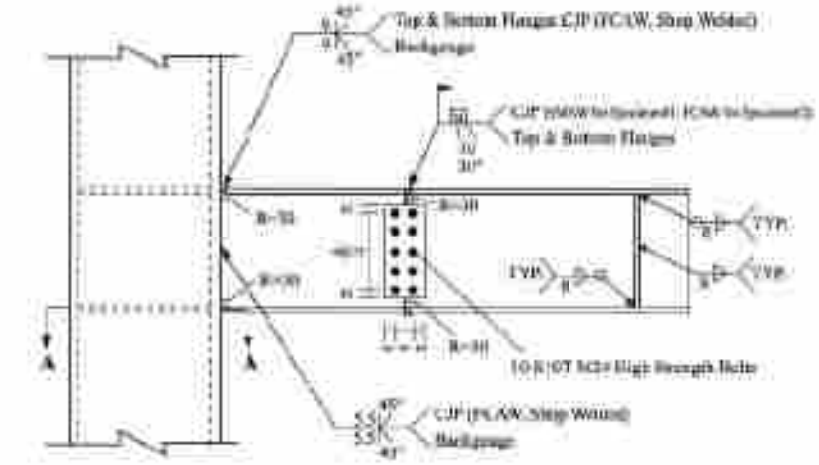

(a) Weld details at web beam, link beam and box column

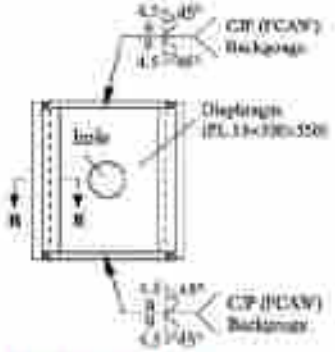

(b) Weld details of section A–A

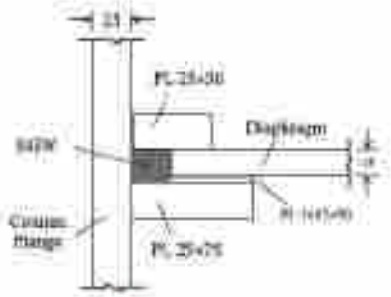

(c) Detail of section B–B

Fig. 6. Weld details in test specimens (unit: mm).

Table 4
Summary of reduction factors of mechanical properties of steels at high temperatures.

Temperature T (°C)	SN400B steel			SM490C FR steel			8.8T bolt		
	$k_y(T)$	$k_u(T)$	$k_E(T)$	$k_y(T)$	$k_u(T)$	$k_E(T)$	$k_y(T)$	$k_u(T)$	$k_E(T)$
25	1.00	1.00	1.00	1.00	1.00	1.00	1.00	1.00	1.00
100	0.92	0.89	0.89	0.95	0.95	0.90	0.90	0.97	0.97
200	0.84	0.84	0.81	0.95	1.00	0.95	0.86	0.96	0.86
300	0.72	0.97	0.77	0.97	1.03	0.92	0.82	0.93	0.77
400	0.62	0.87	0.70	0.93	0.92	0.72	0.65	0.72	0.60
500	0.58	0.62	0.58	0.74	0.75	0.70	0.29	0.44	0.33
600	0.30	0.35	0.35	0.57	0.56	0.35	0.11	0.21	0.13
700	0.17	0.16	0.24	0.28	0.28	0.42	0.01	0.09	0.06
800	0.09	0.11	0.09	0.09	0.09	0.09	0.04	0.07	0.03

[1] $k_u(T) = f_u(T)/f_u$ (25 °C), $k_y(T) = f_y(T)/f_y$ (25 °C), $k_E(T) = E(T)/E$ (25 °C).
[2] f_y = 325–345 MPa for SN400B & SN490C FR at ambient temperature (specified).
[3] f_y = 450–510 MPa for SN400B & SN490C FR at ambient temperature (specified).

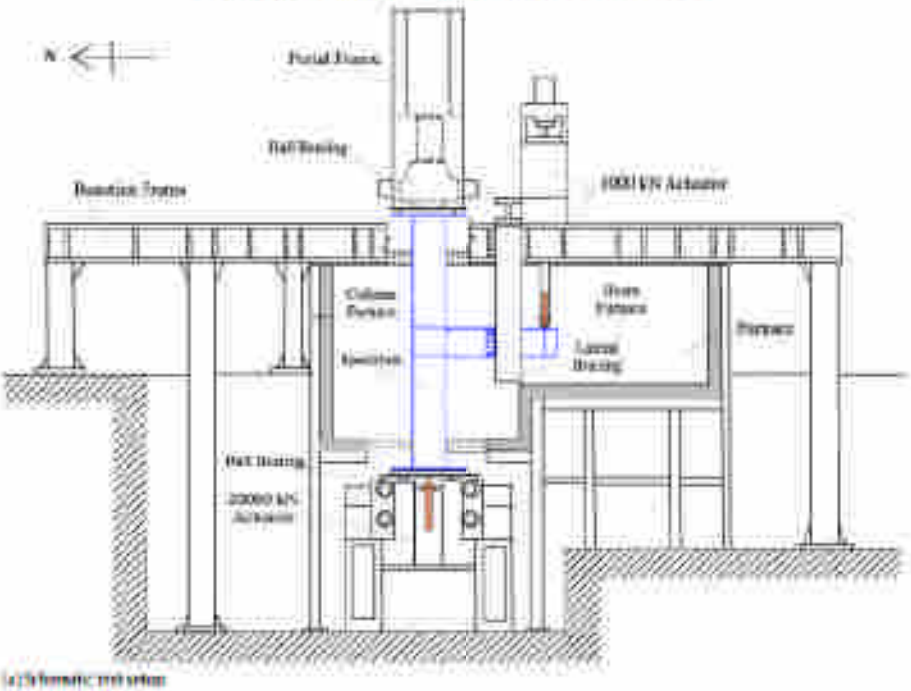

(a) Schematic test setup

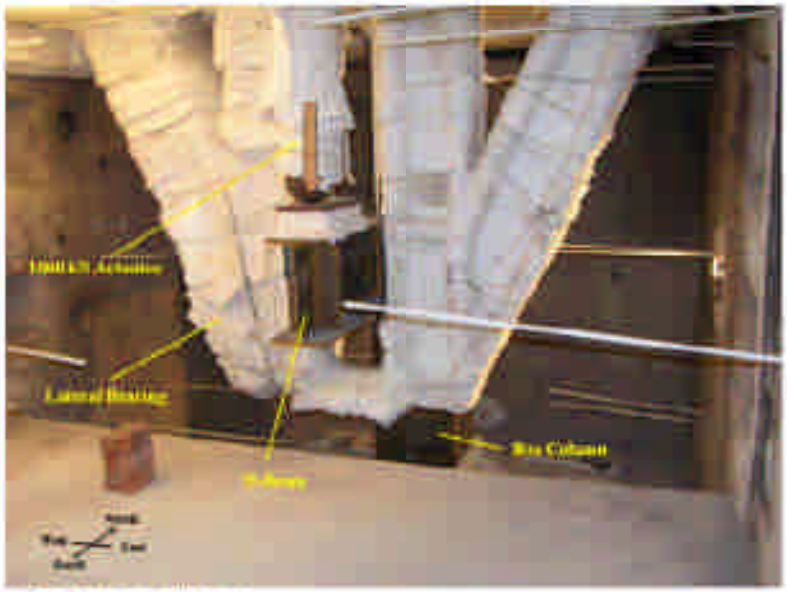

(b) Photo of test setup in the furnace

Fig. 5. Test setup of the fire experiment.

3. Experimental program

3.1. Furnace & loading system

The two specimens were tested using a multi-functional gas furnace at the Fire Experiment Center (ABRI) at Kuei-Jen Campus of National Cheng Kung University. The furnace is composed of two connected sub-furnaces, a column furnace (4 m × 4 m × 3.6 m) and a beam furnace (4 m × 4 m × 2.4 m), as shown in Fig. 5. The furnace is capable of operating the temperature–time heating curves required by the ISO-834 and ASTM-E119 regulations. A 20,000 kN actuator placed underneath the column furnace is combined with

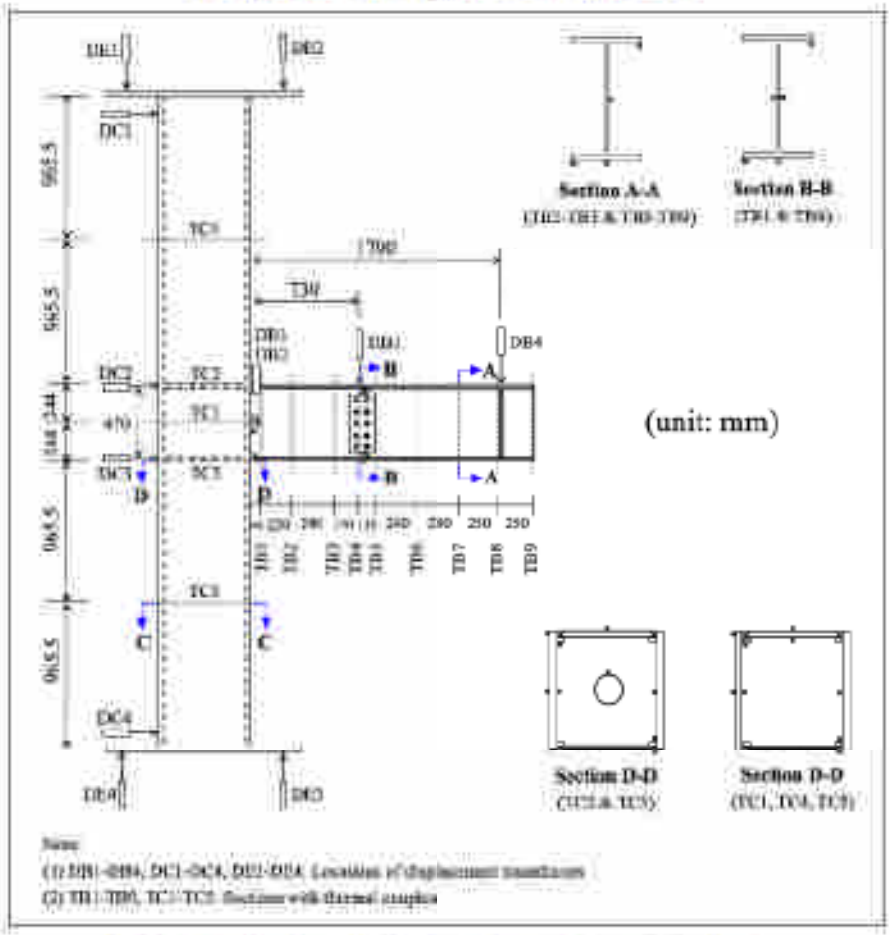

Fig. 6. Locations and numbering of displacement transducers and sections with thermal couples.

Table 5
Chemical composition of SM490A, as the material used.

Chemical composition (%)						
C	Si	Mn	Mo	Nb	V	Ti
0.08	0.23	0.9	0.33	0.024	0.036	0.053

Table 6
Chemical composition of flux-cored JIS Z3313-A1 carbon-molybdenum electrodes.

Chemical composition (%)					
C	Si	Mn	Mo	P	S
0.07	0.50	0.90	0.54	0.013	0.012

a strong portal frame erected above the furnace to provide the required axial force for a test column. Two sophisticated ball-bearing devices are installed on the actuator and the portal frame, respectively, to simulate the hinge boundary conditions for the test column. In addition, several hydraulic rams can be used to create various load combinations for beam loading. The furnace and loading system can be used to test a single structural component of column, beam, or beam-column subassemblies at elevated temperatures.

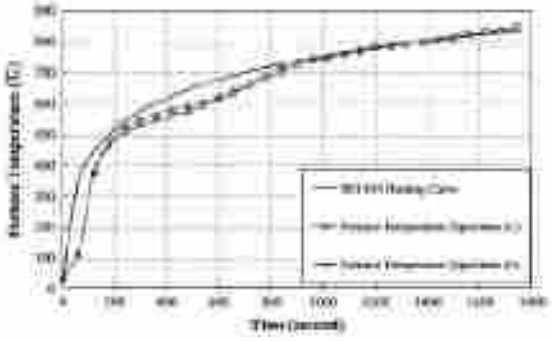

Fig. 7. Furnace temperature–time curves of two fire tests.

3.2. Test setup

The test setup is illustrated in Fig. 5. The box-column of the specimen sat in the center of the column furnace with its two ends connected to the bottom 20,000 kN actuator and the top portal frame through the ball-bearing devices to simulate hinge boundary conditions. The H-beam of the specimen stuck out of

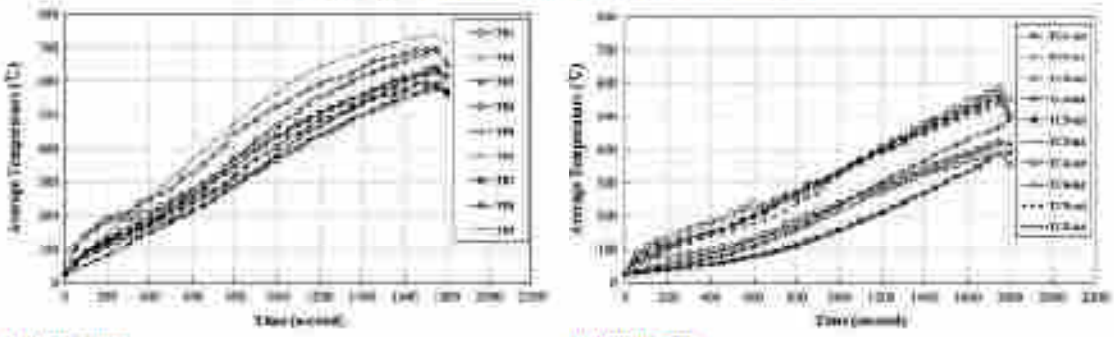

(a) Beam sections. (b) Column sections.

Fig. 5. Sectional temperature variation against time for Specimen #1.

the beam furnace and was laterally braced by a fireproofed steel frame to prevent lateral torsional buckling. Before the fire test, the box-column was loaded with a constant 4900 kN compressive column load from the bottom actuator, and the cantilevered H-beam was point-loaded at a location 1.7 m from the column flange face with a constant downward 360.6 kN beam load. In this test setup, neither the axial restraint nor the reinforced concrete (RC) floor slab was applied to the beam. Without the catenary action at high temperatures developed from the axial restraint and the composite action generated from the RC floor slab, the fire test results of the specimens in this test setup will be more conservative than those with the consideration of the axial restraint and the RC floor slab [13–15].

3.3. Instrumentation for data acquisition

The test data of the two specimens, including temperature distributions, deformations, and the applied loads, were monitored in real-time and recorded throughout the heating process until failure of the moment connection. In order to collect the temperature distributions of the specimens at elevated temperatures, a total of eighty-three K-type thermal couples were TIG welded to each specimen for temperature readings, and were divided into two groups, the IB-section group (TB1–TB9) and the TC-section group (TC1–TC5), to measure the temperature distributions of the H-beam and box-column respectively as shown in Fig. 6. In addition, the furnace temperature distributions were monitored by the furnace control system. Fig. 6 also illustrates that a total of twelve displacement transducers divided into three groups, DB-group (DB1–DB4), DC-group (DC1–DC4) and DE-group (DE1–DE4), were used to observe the structural deformation of each specimen in the fire test. It is noted that the DB4 displacement transducer was placed at the same location as where the beam load was applied, and the DB1 displacement transducer was put at the end of the stub beam. The DC2 and DC3 transducers were used to measure the connection rotation due to column deflection and panel zone deformation.

3.4. Test procedure

In order to compare the fire-resistant performance of Specimens #1 and #2, two fire tests were conducted using the same loading and heating processes for the two specimens. The "constant-load and elevated-temperature" fire test procedure used is briefly described below:

(1) Apply a constant 4900 kN compressive axial load to the box-column of the specimen from the bottom actuator, and maintain the load to the end of the test.
(2) Apply a constant downward 360.6 kN beam load to the cantilevered H-beam end 1.7 m from the column flange face, and maintain the load to the end of the test.
(3) Start burning the furnace according to the ISO-834 temperature–time heating curve.
(4) Unload the constant 360.6 kN beam load when the loading point at the beam end reaches the largest deflection of 500 mm.
(5) Stop the fire in the furnace and unload the constant 4900 kN column load.

4. Test results

4.1. Temperature measurements

Fig. 7 plots the ISO-834 heating curve and the two curves of average furnace temperature against time recorded from the two fire tests for comparison. The average furnace temperatures of the two fire tests were somewhat lower than the ISO-834 temperature before 800 s, and the relative errors were within 10%. However, the average furnace temperatures of the two fire tests after 800 s increased and matched the ISO-834 curve until the termination of each fire test. The furnace heating in the fire test of Specimen #1 lasted for 1790 s and reached a maximum temperature of 843.5 °C. In the fire test of Specimen #2, the furnace was heated for 1350 s with a maximum temperature of 826.7 °C. Therefore, Specimen #1, with the fire-resistant stub beam, was able to resist deformation about 200 s longer than Specimen #2 (the normal steel stub beam in fire).

Figs. 8 and 9 show the temperature variations of the beam and column sections against time for Specimens #1 and #2 during the fire tests. It can be seen that the temperature distributions of the two specimens are somewhat different, but the average furnace temperatures for the two fire tests are very close. This is because the furnace control system heats up the furnace according to the average furnace temperature of the working furnace thermal couples. The control system will discard the broken furnace thermal couples and continue to operate according to the average temperature computed from the other furnace thermal couples which are working. As a result, the local furnace temperatures of the two fire tests may not be the same, and that causes the sectional temperature differences of the two specimens. The average temperatures of the beam sections (TB1–TB9) and column sections (TC1–TC5) were simultaneously raised as the furnace temperature increased. However, the temperature distribution of each specimen varied from section to section. Compared to the box-column, the H-beam was easier to heat because of the shape of the open section and the thinner flange and web plates. For the H-beam, the lower temperature distributions occurred at the beam-to-column connection

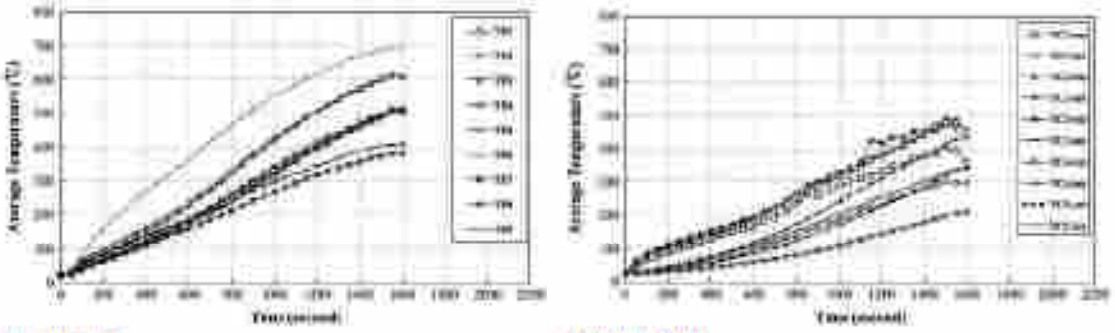

(a) Beam sections (b) Column sections

Fig. 9. Sectional temperature variation against time for Specimen #2.

(a) Specimen #1 after fire test (b) Specimen #2 after fire test

Fig. 10. Photos of the two specimens after fire test.

(TB1) and the beam sections (TB4–TB8) close to the lateral bracing frame, which acted as a heat transfer barrier. The highest temperature distribution was located at the H-beam end (TB6). The second highest temperature was distributed at the TB2 section, where bottom flange local buckling (FLB) occurred. Comparing the temperature data presented in Figs. 8 and 9, Specimen #1 can resist higher temperature in the fire test than Specimen #2.

4.2. Determination of critical temperature (T_{cr})

Fig. 10 shows photos of the two specimens after the fire tests. Both of the specimens failed at the moment connections because of the strength degradation of steel at elevated temperatures. Since the H-beams of the two specimens were firmly braced in the fire tests, the two H-beam to box-column moment connection specimens successfully reached their plastic moments (M_p) in fire and then failed in the same mode of bottom flange local buckling followed by web buckling due to large inelastic deformation. In addition, no damage or large deformation was observed in the box columns and the spliced connections between the stub and hot beams. No fracture occurred at the CJP welds between the beam and the column flanges.

Since high temperature affects the strength and deformation of steel, the failures of the two specimens are influenced by the temperatures distributed in their H-beams. Fig. 10 shows that the critical temperature (T_{cr}), which causes the failure of the moment connection, of Specimens #1 or #2 is located at the beam portion where bottom flange local buckling occurs, and Fig. 8 shows that the beam section TB2 is the closest section to the portion of flange local buckling. The thermocouples in section TB2 measure the closest critical temperature data for the two specimens. The research group discovered that the critical temperature can be precisely determined by plotting a graph of the relationship between the connection rotation and the average temperature of TB2 beam section during the fire test. The connection rotation can be computed from the test data recorded in the DC2 and DC3 transducers, as follows:

$$\theta_c = \frac{(\delta_{DC2} - \delta_{DC3})}{h} \quad (1)$$

where θ_c = rotation of the beam-to-column connection; δ_{DC2} = displacement measured from the DC2 displacement transducer; δ_{DC3} = displacement measured from the DC3 displacement transducer; and h = distance between transducers DC2 and DC3 (470 mm, see Fig. 6).

Fig. 11(a) illustrates the variation of connection rotation against the average temperature of TB2 beam section for Specimen #1. As the temperature increased in the box-column, the flexural stiffness of the box-column decreased, which caused the connection rotation to increase. The connection rotation plunged sharply when it reached its peak value of 1.9×10^{-3}. This sudden change in connection rotation was due to the occurrence of flange local buckling in the bottom flange of H-beam. The buckled beam-to-column

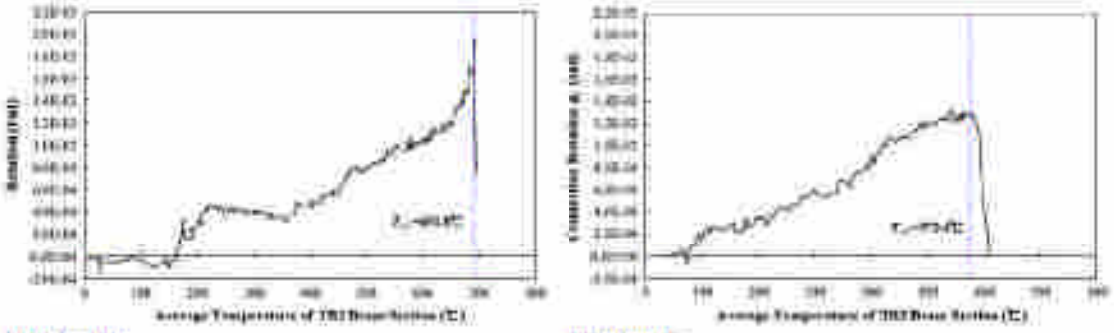

(a) Specimen #1. (b) Specimen #2.

Fig. 11. Connection rotation due to column deflection vs. average temperature of TB2 beam section.

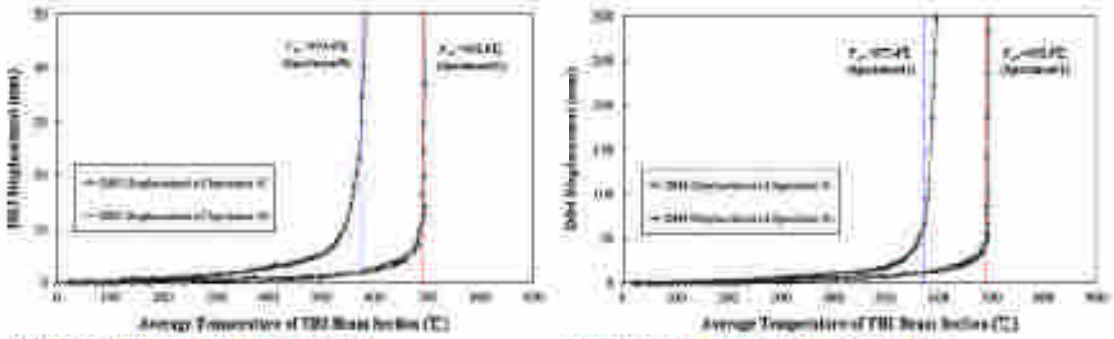

(a) DB3 location (710 mm away from the column face). (b) DB4 location (1550 mm away from the column face).

Fig. 12. Displacement vs. average temperature of TB2 beam section for two specimens.

moment connection could no longer transfer moments from the H-beam to the box-column, so the box-column deflection and connection rotation bounced back. The temperature of 692.8 °C in section TB2, corresponding to the peak connection rotation (1.8×10^{-2}), can be used to represent the critical temperature of Specimen #1. Using the same graphical method in Fig. 11(b), the critical temperature of 573.4 °C corresponding to the peak connection rotation (1.3×10^{-2}) can be determined for Specimen #2. Therefore, Specimen #1 resisted a 120 °C higher critical temperature than Specimen #2. Fire-resistant steel enhances the fire-resistant performance of the H-beam to box-column moment connection.

4.3. Displacement measurement

Fig. 12 shows the fire test data on H-beam displacements against the average temperature of TB2 section at the DB3 and DB4 locations for the two specimens. The critical temperatures of the two specimens determined from the previous section are plotted as well. Due to the flexural-stiffness reduction of the H-beam at elevated temperatures and the constantly applied beam end moment, the beam displacements at DB3 and DB4 for Specimen #2 increased gradually before the TB2 temperature reached about 500 °C. When the TB2 temperature exceeded about 500 °C, the H-beam of Specimen #2 started to deform more and faster. A sharp increment in displacement occurred at locations DB3 and DB4 of Specimen #2 as the TB2 temperature approached the critical temperature (573.4 °C), at which temperature the H-beam of Specimen #2 became unstable and could no longer resist the constantly applied beam load (350.0 kN). Meanwhile, Specimen #1 remained stable and the DB3 and DB4 displacements of Specimen #1 were much smaller than those of Specimen #2, indicating that the fire resistant stub beam had stronger flexural stiffness than the stub beam made of normal structural steel. The DB3 and DB4 displacements of Specimen #1 increased steadily until the TB2 temperature approached the critical temperature of 692.8 °C. Steep increments of the displacements were observed at the critical temperature of 692.8 °C.

5. Numerical simulation

Due to the complicated behaviors of beam-to-column connections in fire, most researchers have used the finite element (FE) method as the powerful tool for numerical simulations. Several three-dimensional (3-D) nonlinear FE models have been proposed to analyze the behaviors of beam-to-column connections at elevated temperatures [16–19]. In this study, a general-purpose finite element implicit solver, ABAQUS/Standard, was employed to perform 3-D nonlinear FE simulations for the two specimens at elevated temperatures in the furnace. As shown in Figs. 8 and 9, the average temperature–time history of each cross section collected from the fire tests was assigned to its associated temperature block (see Fig. 13) in the FE model of each specimen as the predefined temperature distributions. For the 3-D nonlinear FE structural analyses in ABAQUS/Standard, both material and geometric nonlinearities were considered. The high-temperature stress–strain relationships of SN490B steel, SN490C-FR fire-resistant steel, and SHDT bolts obtained from the high-temperature tensile coupon tests, as well as the von Mises yield criterion and the associative flow rule, were adopted to model the material nonlinearities of the two specimens. Geometric nonlinearity was also taken into

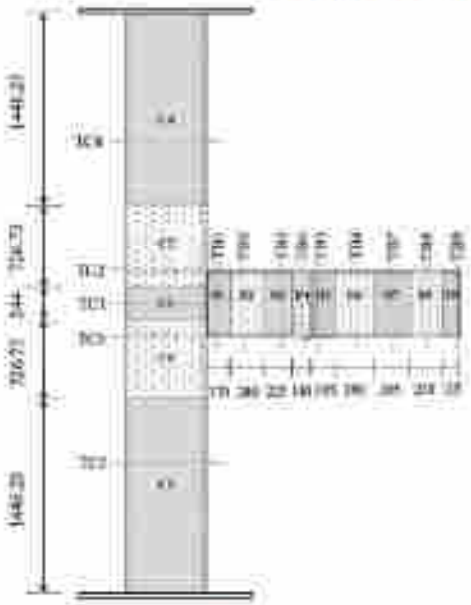

Fig. 13. Temperature blocks of test specimen for FE analysis.

consideration by activating the optional parameter "NLGEOM" in ABAQUS/Standard to capture the large deformation and local instability effects in the 3-D FE models of the two specimens.

5.1. FE modeling

5.1.1. FE meshing & element type

The specimen was divided into five groups of components for the 3-D FE meshing and modeling, including the box column, stub H-beam, link H-beam, two splice plates, and ten bolts, as shown in Fig. 14. The welded connections between components were simulated using the "tie" type constraint in ABAQUS. The two splice plates and ten bolts are used to splice the webs of the stub beam and link beam as a splice connection, which has detailed contact modeling among the bolts, splice plates, and beam webs. In the 3-D FE modeling, all of these components were precisely created according to their original design dimensions and were neatly meshed using the 3-D hexahedral solid (brick) elements. The 3-D 8-node first order solid elements with incompatible modes, designated as C3D8I in ABAQUS, were used for the entire FE model of the two specimens. In addition to having three displacement degrees of freedoms at each node as the standard first-order solid elements, a linear C3D8I solid element with full integration ($2 \times 2 \times 2$ Gauss points) has thirteen additional degrees of freedom to remove the shear-locking problem. Using the incompatible mode elements can obtain results comparable to quadratic elements, and can also save computation time. Table 7 shows the element and node numbers of the specimen components in the 3-D FE modeling.

5.1.2. Contact modeling

In order to simulate realistic behavior of the splice connection joining the stub beam web and the link beam web, detailed contact modeling was built at the contact surfaces of beam webs, splice plates, and bolts as shown in Fig. 15. The contact surfaces within the connection occurred at the interfaces of the following contact pairs: the bolt heads and splice plates, the bolt shanks and splice plates, the bolt shanks and beam webs, the bolt nuts and splice plates, and the splice plates and beam webs. Hence, a total of fifty-four contact relationships were created in the numerical simulation of the splice connection. These contact relationships were all defined as "surface-to-surface" contacts in ABAQUS/Standard, and the small-sliding option was used for the sliding formulation. The contact surfaces on the bolt head, bolt shank, and bolt nut were all defined as master surfaces, and the surfaces contacted with the bolts were defined as slave surfaces. For the splice plate–beam web contact pairs, the contact surfaces on the splice plates were defined as master surfaces and those on the beam webs were defined as slave surfaces. The contact behavior in the normal direction for each contact pair was modeled as a "hard contact." For the contact behavior in the tangential direction, the isotropic Coulomb friction model with the use of the penalty method was used for each contact pair.

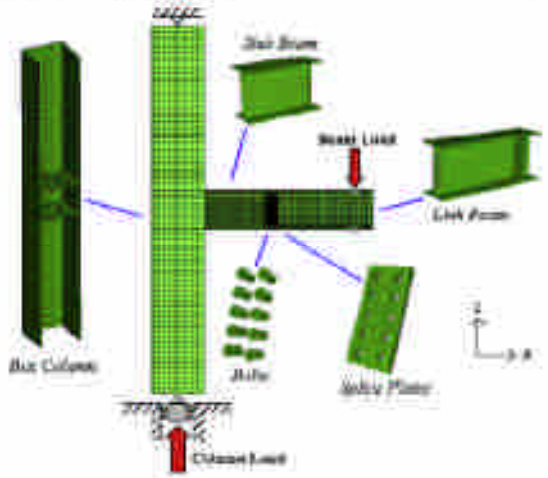

Fig. 14. FE meshing and modeling for test specimens.

Table 7
Node and element numbers of specimen components in FE modeling

Component	Node number	Element number
Column	6932	6024
Stub beam + Link beam	18331	13442
Splice plate (×2)	6010 × 2	5384 × 2
Bolt (×10)	798 × 10	576 × 10

5.1.3. Boundary conditions

In order to simulate the hinge boundary condition at the top column end, the center of the top column end in the FE model was restrained against rotation about the longitudinal axis of the box-column (R_z) and translations in all three directions (U_x, U_y, U_z). A similar boundary condition was applied to the bottom end of the box-column in the FE model, except that the restraint against translation in the axial direction (U_z) was released to simulate the roller boundary condition. A constant 4900 kN compressive axial load was applied to the box-column from the bottom end. To prevent lateral torsional buckling of the H-beam, the restraints against lateral translation (U_x) of the H beam were placed at the location (1.7 m from the column face) where the downward constant beam load (360.6 kN) was applied.

5.1.4. Material properties

The high-temperature stress–strain relationships of SN490B steel, SN490C-HR fire-resistant steel, and S10T high strength bolts

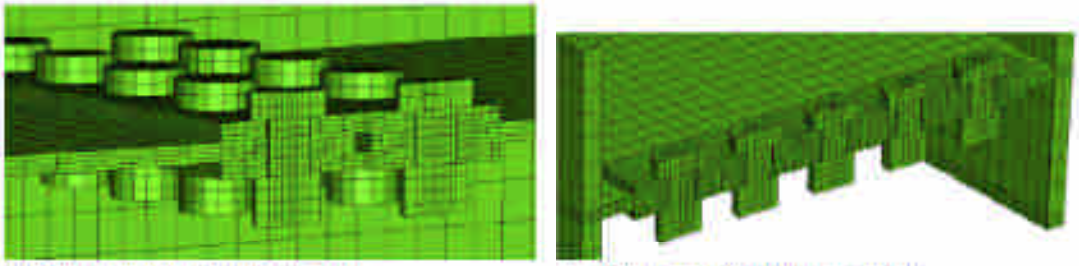

(a) 3-D cross section view of the splice connection (I).

(b) 3-D cross section view of the splice connection (II).

Fig. 15. FE modeling for the splice connection joining the stub and bit beams.

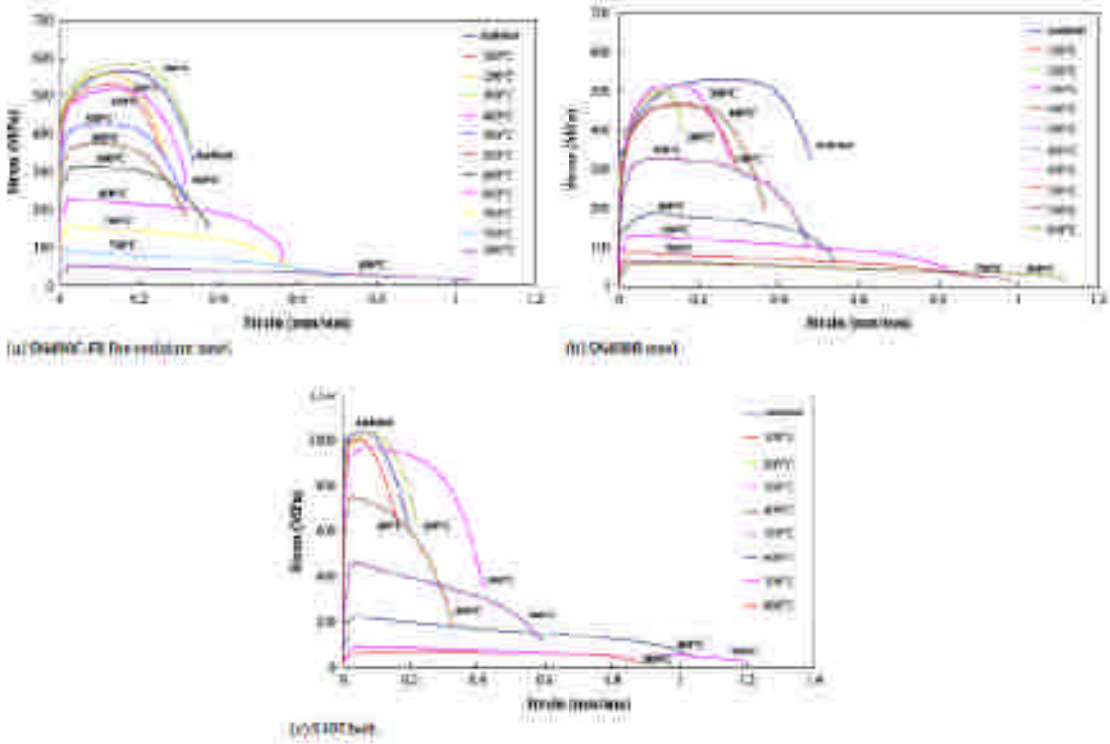

(a) SM490C FE fire resistance test.

(b) SM490B test.

(c) S355 bolt.

Fig. 16. Stress–strain relationships of SM490C FE, SM490B and S355 steels at high temperatures.

(see Fig. 16) obtained from the high-temperature tensile coupon tests in the materials lab of the steel provider were used to model the material properties of the two specimens for the 3-D nonlinear FE structural analysis. In ABAQUS/Standard, the engineering stress–strain relationships read from the tensile coupon test data had to be converted to the true stress–strain relationships for the input.

5.2. Numerical results of FE analyses

Figs. 17 and 18 compare the photos of the damaged specimens after fire with the photos of the FE simulation results of connection failures for Specimens #1 and #2, respectively. The photos show that the proposed 3-D FE model successfully simulate the failure modes of bottom flange local buckling and web buckling at the moment connection portions of the two specimens.

Fig. 19 compares the FE analysis results of connection rotation against the temperature in section TB2 with the experimental data for the two specimens. The FE analysis results also predict the critical temperatures for the two specimens using the graphical method described in Section 4.2, as plotted in the figures. Table 6 lists the critical temperatures predicted from the FE analysis results and compares them with the critical temperatures obtained from the fire tests for the two specimens. For Specimen #1, as shown in Fig. 19(a), the FE simulated connection rotation against TB2 section temperature match well with the test data, and the FE predicted critical temperature (673.5 °C) is very close to the test critical temperature (692.8 °C), with a relative error of −1.8%. Fig. 19(b) compares the FE simulated and experimental results of connection rotation versus TB2 temperature for Specimen #2. The FE simulated connection rotation is somewhat lower than the experimental results, but the critical temperature (598.9 °C)

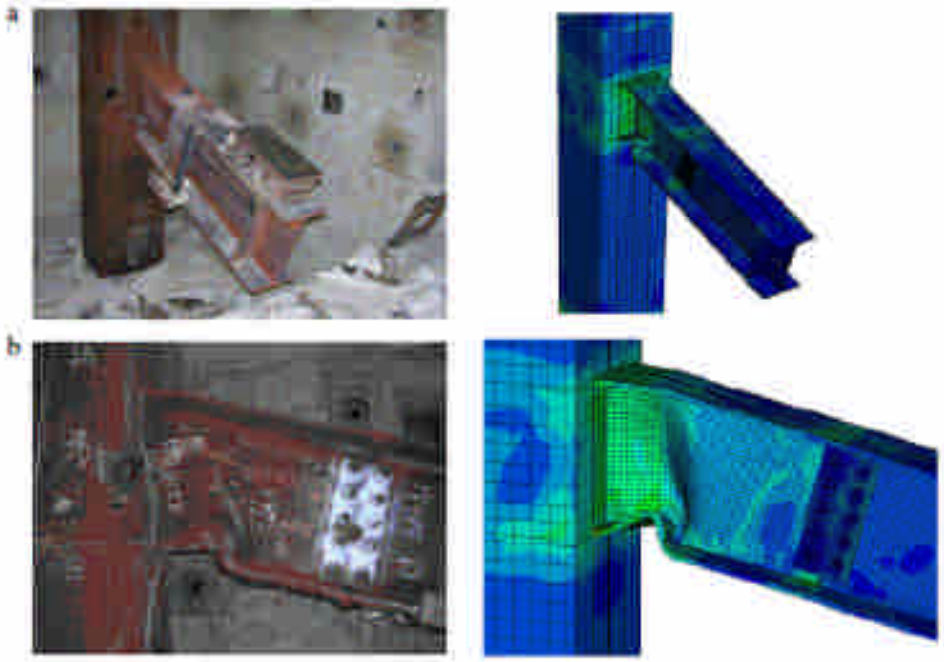

Fig. 17. Comparison of the FE simulated failure mode with the test result for Specimen #1.

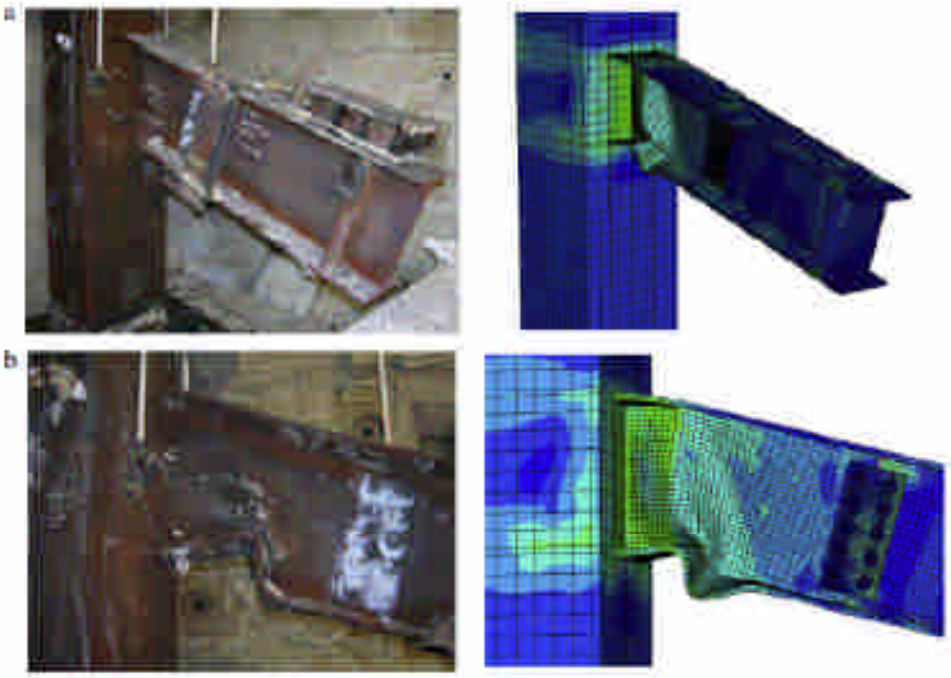

Fig. 18. Comparison of the FE simulated failure mode with the test result for Specimen #2.

Table 6
Experimental and FE predicted critical temperatures for two specimens.

Specimen number	Beam load (kN)	Beam end moment produced by beam load (kN m)	Critical temperature (T_{cr})		
			Test result	FE analysis	Error
#1	360.0	613.1 (44% $M_{p,ambient}$)	602.8 °C	573.4 °C	(−4.88%)
	408.4	394.3 (49% $M_{p,ambient}$)	–	524.4 °C	–
#2	360.6	613.1 (49% $M_{p,ambient}$)	573.4 °C	536.9 °C	(6.4%)

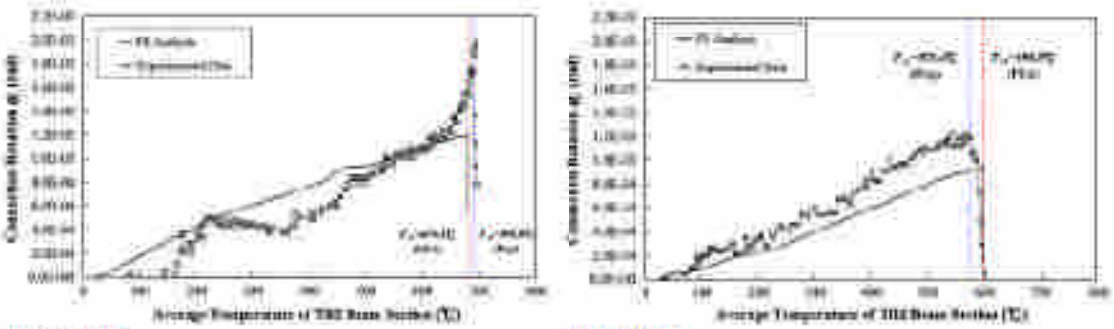

(a) Specimen #1. (b) Specimen #2.

Fig. 19. Comparison of the FE simulated and experimental results for connection rotation vs. average temperature of TB2 beam section.

obtained from the FE result still provides a good prediction for the test critical temperature (573.4 °C), with a relative error of 4.4%.

Fig. 20(a) and (b) compare the FE simulated and experimental DB4 beam-end displacement results for specimens #1 and #2, respectively. As can be seen, the proposed 3-D FE model provides a fairly good simulation of the DB4 beam-end displacement against the elevated TB2 temperature. When the two FE simulated DB4-displacement curves of the two specimens reach their own FE predicted critical temperatures, both curves go up steeply. The trends of both curves closely resemble that of the test data.

5.3. Comparison of two specimens under a constant bending moment of 49% $M_{p,ambient}$

According to the realistic yield strengths of SN490C-FR and SN490B steels shown in Table 3, the computed plastic moments at ambient temperature ($M_{p,ambient}$) for the H-beams of Specimens #1 and #2 are 1405.7 kN m (F_y = 440.1 MPa and Z_x = 3.11 × 10^3 mm^3) and 1247.4 kN m (F_y = 386.6 MPa and Z_x = 3.11 × 10^3 mm^3), respectively. Therefore, the applied constant beam load of 360.6 kN produces the constant beam end moment of 613.1 kN, which equals 44% $M_{p,ambient}$ of Specimen #1 and 49% $M_{p,ambient}$ of Specimen #2. For a further comparison, a new 3-D FE analysis for Specimen #1 was performed and the original constant beam load (360.6 kN) applied to Specimen #1 was replaced by 408.4 kN to generate the beam end moment equal to 49% $M_{p,ambient}$ of Specimen #1. The new FE analysis result of Specimen #1 was then compared to the original FE analysis result of Specimen #2 under a beam end moment equal to 49% $M_{p,ambient}$. Fig. 21 compares the FE simulated DB4 displacement curves and the FE predicted critical temperatures for the two specimens. The numerical comparison shows that even though each specimen was subjected to a constant beam end moment of 49% of its own H-beam plastic moment, Specimen #1 still had a better fire-resistant performance and higher critical temperature than Specimen #2. Table 6 summarizes the experimental and FE predicted critical temperatures obtained for the two specimens in this study.

6. Conclusions

The proposed method of using fire-resistant steel in the stub beams of column-tree moment connections can effectively enhance the fire-resistance of beam-to-column moment connections, including the capability to resist the fire-induced thermal-induced structural deformation, and increase the critical temperature that causes the structural component to fail. In addition, using fire-resistant steel only in the crucial connection portion instead of applying it to the whole beam can reduce expenses, since the cost of fire-resistant steel is higher than that of conventional structural steel. The superior fire-resistant performance obtained using the proposed method was verified in this study by testing two full-scale column-tree moment connection specimens at elevated temperatures according to a standard ISO-834 fire. The important experimental quantities of the two specimens in the fire tests, such as furnace temperatures, specimen temperature distributions, and structural deformations, were successfully measured using the designed instrumentations and were systematically compared in this study. In order to simulate the test results numerically, a highly detailed 3-D nonlinear FE model was developed in this study to simulate the structural behaviors of the two specimens in fire. The numerical results obtained from the 3-D nonlinear FE analyses for the two specimens agree well with the respective experimental results. The FE analysis results show that whether the two specimens are subject to the same beam end moment or to a beam end moment equal to the same percentage of their own H-beam plastic moment, the specimen with the moment connection portion (i.e., the stub beam) made of fire-resistant steel has the better fire-resistant performance than the specimen with the moment connection portion made of normal structural steel. With the developed 3-D nonlinear FE model, more comprehensive investigations and further parametric studies for the H-beam to box-column moment connections can be conducted in the future.

Acknowledgements

The authors gratefully acknowledge the assistance and support from the Architecture and Building Research Institute (ABRI), Ministry of the Interior, Taiwan, the China Steel Corporation and the Tung Ho Steel Enterprise Corporation.

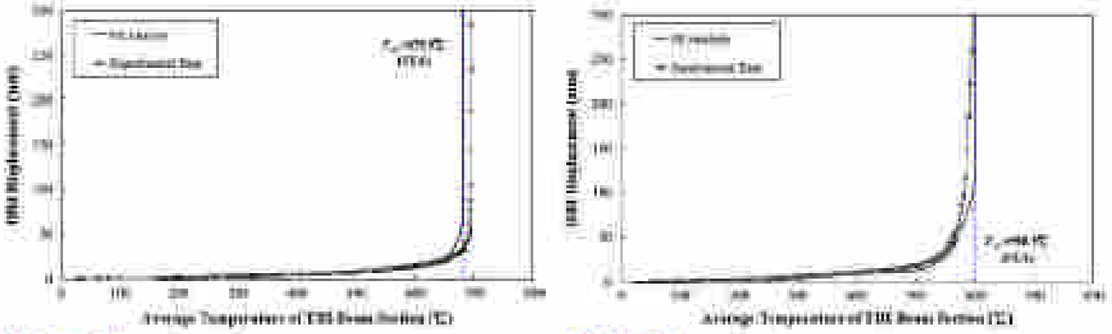

(a) Specimen #1.

(b) Specimen #2.

Fig. 20. Comparison of the FE simulated and experimental results for OM displacements vs. average temperature of TBB beam section.

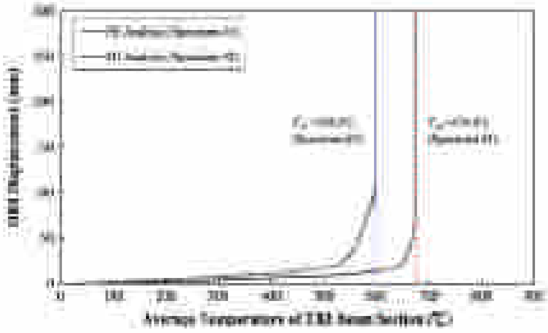

Fig. 21. Comparison of the FE simulated OM displacements for the two specimens under the constant bending moment equal to [illegible]

References

[1] NIST. Final report on the collapse of the World Trade Center towers. Report NIST NCSTAR 1. National Institute of Standards and Technology, Gaithersburg Maryland (USA); 2005.

[2] FEMA. World Trade Center building performance study: Data collection, preliminary observations and recommendations. FEMA-403. Washington, DC (USA): Federal Emergency Management Agency; 2002.

[3] Newman GM, Robinson JT, Bailey CG. Fire safety design: A new approach to multi-storey steel framed buildings. Ascot, Berkshire (UK): SCI Publication P288; 2000.

[4] Lawson RM. Fire engineering design of steel and composite buildings. J Const Steel Res 2001;57(12):1233–47.

[5] Sakumoto Y, Yamaguchi T, Ohashi M, Saito H. High-temperature properties of fire-resistant steel for buildings. J Struct Engrg 1992;118(2):392–407.

[6] Kelly FS, Sha W. A comparison of the mechanical properties of fire-resistant and S275 structural steels. J Const Steel Res 1999;50(3):223–33.

[7] Leston-Jones LC, Lennon T, Plank RJ, Burgess IW. Elevated temperature moment-rotation tests on steelwork connections. Proc Inst Civ Eng Struct Bldgs 1997;122(4):[illegible]

[8] Al-Jabri KS, Lennon T, Burgess IW, Plank RJ. Behaviour of steel and composite beam-column connections in fire. J Const Steel Res 1998;46(1–3): [Paper no. 180].

[9] Wang WY, Li GQ, Dong YL. Experimental study and spring-component modelling of extended end-plate joints in fire. J Const Steel Res 2007;63(8): 1127–37.

[10] Ding J, Wang YC. Experimental study of structural fire behaviour of steel beam to concrete filled tubular column assemblies with different types of joints. Eng Struct 2007;29(12):3485–502.

[11] Qian ZH, Tan KH, Burgess IW. Behavior of steel beam-to-column joints at elevated temperature: Experimental investigation. J Struct Eng 2008;134(5): 713–26.

[12] Yu H, Burgess IW, Davison JB, Plank RJ. Experimental investigation of the behaviour of fin plate connections in fire. J Const Steel Res 2009;65(3):723–36.

[13] Liu TCH, Fahad MK, Davies JM. Experimental investigation of behaviour of axially restrained steel beams in fire. J Const Steel Res 2002;58(9):1211–30.

[14] Yin YZ, Wang YC. Analysis of catenary action in steel beams using a simplified hand calculation method, Part 1: Theory and validation for uniform temperature distribution. J Const Steel Res 2005;61(2):183–211.

[15] Liu TCH. Moment-rotation-temperature characteristics of steel/composite connections. J Struct Engrg 1999;125(10):1188–97.

[16] Liu TCH. Three-dimensional modelling of steel/concrete composite connection behaviour in fire. J Const Steel Res 1998;46(1–3):319–20.

[17] Al-Jabri KS, Seibi A, Karrech A. Modelling of unstiffened flush endplate bolted connections in fire. J Const Steel Res 2006;62(1–2):151–9.

[18] Sarraj M, Burgess IW, Davison JB, Plank RJ. Finite element modelling of steel fin plate connections in fire. Fire Saf J 2007;42(6–7):408–15.

[19] Yu H, Burgess IW, Davison JB, Plank RJ. Numerical simulation of bolted steel connections in fire using explicit dynamic analysis. J Const Steel Res 2008; 64(5):515–25.